Wideband High-Gain Millimetre-Wave Three-Layer Hemispherical Dielectric Resonator Antenna

Abdulmajid A. Abdulmajid[1, 2, *], Salam Khamas[2], and Shiyu Zhang[3]

Abstract—A wideband high gain three-layer hemispherical dielectric resonator antenna (HDRA) that operates at TE_{511} and TE_{711} higher order modes is proposed. The HDRA is composed of three layers, which has permittivities of 20, 10, and 3.5. The multilayer structure has been chosen in order to reduce the Q-factor and achieve a wider impedance bandwidth. Cross slot feeding mechanism has been utilized taking into account the excited higher order modes for gain enhancement. The proposed antenna provides an impedance bandwidth of 35.8% over a frequency range of 20.8 to 29.9 GHz in conjunction with a high gain of ~ 9.5 dBi. The proposed DRA represents the first attempt in utilizing a mm-wave hemispherical DRA.

1. INTRODUCTION

Millimetre-wave frequencies are receiving increased research attention due to potential applications in 5G communication systems. However, antenna designs face a number of challenges at the mm-wave frequency range such as a considerable attenuation that necessitates the utilization of a high gain antenna. On the other hand, the well-known directive horn antenna suffers from a number of drawbacks at the mm-wave frequency range such as high cost and a relatively large size which make such antennas less desirable [1, 2]. In addition, arrays are associated with potentially high Ohmic losses in the feed networks at those frequencies [3]. Furthermore, microstrip antennas have well-known limitations such as narrow impedance bandwidths of 2–5% and considerably lower radiation efficiencies [4]. Therefore, a DRA represents a suitable choice to address the aforementioned limitations as it offers an enhanced gain in conjunction with high radiation efficiency as well as other appealing features such as small size, various shapes, easy excitation, low profile, and light weight [5, 6].

The impedance bandwidth can be significantly increased by the addition of a dielectric coat that acts as a transition region between the antenna and free space. Recently, it has been reported that coating the DRA can also improve the gain and circular polarisation as well as impedance bandwidths [7, 8]. Furthermore, wideband multi-layer hemispherical DRAs have been reported in [9] utilizing a slot aperture feed, where a bandwidth of 55% has been achieved by exciting TE_{111} and TE_{221} resonance modes. In addition, a coaxial probe fed three-layer hemispherical DRA has been proposed using materials with relative permittivities of 9, 4, and 3 for the inner, middle, and outer layers, respectively, where a bandwidth of 65.6% has been achieved in conjunction with a lower gain of 3.2 dBi when the lower order modes of TM_{101} and TM_{102} are excited [10]. Another three-layer hemispherical DRA has been reported, where it has been demonstrated, through optimization of the outer layer's permittivity, that a broadband coupling can be established to provide impedance bandwidth and gain of 9.6% and 6.4 dBi by exciting the TE_{113} mode [11]. In an alternative study, a wide impedance bandwidth of

$\sim 25\%$ has been measured when a conformal strip is used to feed a three-layer hemispherical DRA that supports the TE_{111} lower order mode [12]. Furthermore, an alternative design of a slot-coupled three-layer HDRA has provided wide impedance bandwidth of 29% and gain of 4.4 dBi when the TE_{111} resonance mode is excited [13]. Comparison of the performance of a two-layer hemispherical DRA with that of a single layer counterpart has demonstrated a wider bandwidth of 31.9% in conjunction with a modest gain of 2.5 dBi for the two layer hemispherical DRA compared to a bandwidth of 14% for single layer DRA operating at the lower order mode of TM_{101} [14]. However, although the previous investigations of multi-layer hemispherical DRAs have concentrated on bandwidth enchantment, no previous investigation has been conducted on multilayer HDRA neither for gain enchantment nor for mm-wave band operation. It is the aim of this paper to address the gain and impedance bandwidth enhancements when a cross-slot is utilized to feed a multilayer hemispherical DRA that operates in the mm-wave frequency range.

2. HEMISPHERICAL DRA CONFIGURATION

As illustrated in Fig. 1, a hemispherical DRA geometry is defined by radius a and dielectric constant ϵ_r. As a result, the DRA resonance modes are exclusively dependent on those two parameters. In addition, HDRAs can support two types of modes based on the chosen feed mechanism. For example, when the hemispherical DRA is fed using a slot aperture, transverse electric modes (TE_{pmn}) will be excited [15]. On the other hand, transverse magnetic (TM_{pmn}) field modes will be achieved when the hemispherical DRA is fed using a probe [16]. The mode indices p, m, and n denote the variation of the fields in the radial, r, azimuth, ϕ, and elevation, θ, directions, respectively. Furthermore, the lowest order TE mode is TE_{111}, which is equivalent to a short horizontal magnetic dipole, while TM_{101} represents the lowest order TM mode, and it is equivalent to a short electric monopole [17]. In this study, the CST MWS eigen mode solver [18] has been utilized to investigate the modes due to the complexity of the required equations. The relative permittivities of the inner, middle, and outer layers are chosen as $\epsilon_{r1} = 20$, $\epsilon_{r2} = 10$, and $\epsilon_{r3} = 3.5$, respectively. These dielectric constants are chosen in order to achieve wide bandwidth and high gain combination. The feeding cross-slot's arm lengths and widths are optimised, using the CST parametric sweep, as $ls_1 = ls_2 = 4$ mm and $ws_1 = ws_2 = 1.35$ mm.

(a)   (b)
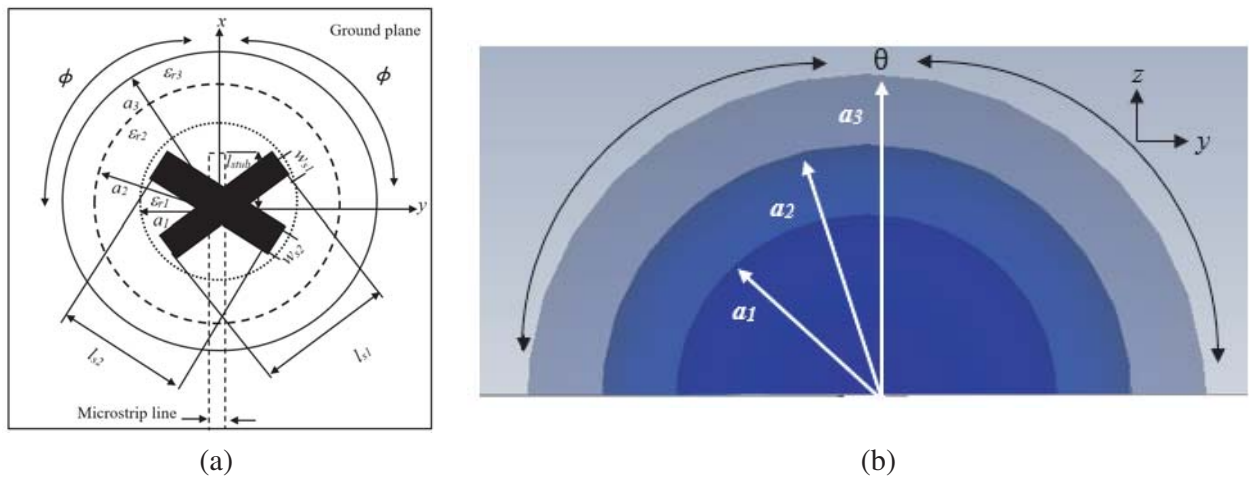
Figure 1. A three-layer hemispherical DRA excited by cross slot (a) top view, (b) side view.

3. ANTENNA DESIGN AND ANALYSIS

It is well known that higher order modes DRAs offer higher gain [19]. However, these modes are associated with higher effective permittivity, hence a narrower impedance bandwidth is expected. In this study, a DRA element with a high permittivity has been chosen for size reduction purposes. The

DRA has been coated by two layers in order to provide a multi-stage transition region between free space and the DRA element with minimised wave reflections at all interfaces, which results in wide bandwidth while maintaining the high gain.

3.1. Single Layer HDRA

A single layer higher order mode hemispherical DRA is investigated in this section using a relative permittivity of 10 and radius of 11 mm. With reference to Fig. 2, it can be observed that the proposed antenna supports the following higher order resonance modes: TE_{911}, $TE_{11,11}$, and $TE_{13,11}$ at 21.3 GHz, 24.6 GHz, and 29.5 GHz, respectively, which provide respective impedance bandwidths of 3.3%, 2.4% and 2.7% as well as gains of 6.8 dBi, 8.8 dBi and 10.7 dBi, respectively. In addition, the DRA has also been simulated with a size of 15 mm to excite the $TE_{15,11}$ mode at 28.6 GHz which offers an enhanced gain of 11.2 dBi in conjunction with a narrow impedance bandwidth of 0.1%. As expected, the achieved high gain is associated with a narrow bandwidth. Furthermore, the DRA footprint is relatively large and may impose a limit on the applicability of the proposed high gain DRA. Therefore, a higher DRA relative permittivity of 20 with a radius of 4.5 mm has been considered in order to design a physically smaller DRA with high gain. The reflection coefficient is presented in Fig. 3, where it can be noted the TE_{511} and TE_{711} modes are excited at 21.5 GHz and 28.5 GHz, with impedance bandwidths of 5.46% and 4.5% and identical gain of 10 dBi for both modes. It should be noted that these bandwidths are wider than those of Fig. 2, which can be explained as a result of exciting lower order modes due to the smaller DRA size.
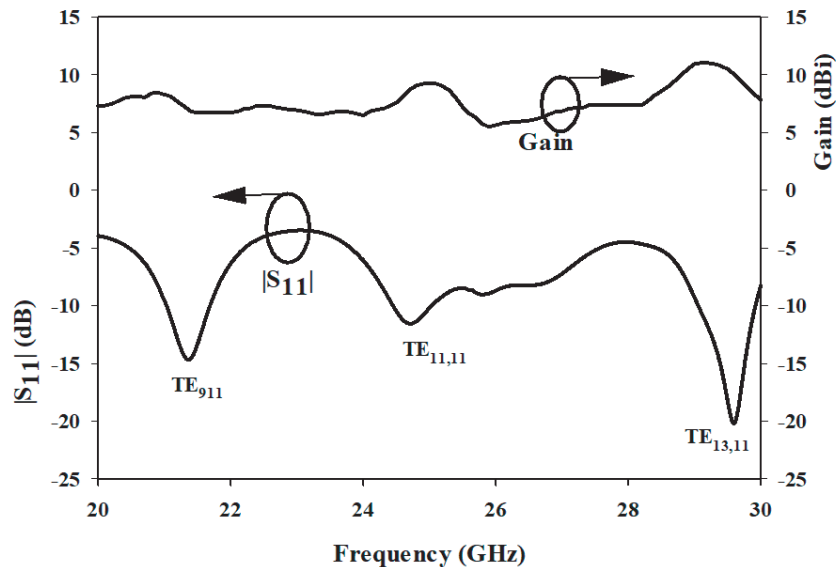

Figure 2. Reflection coefficient and gain of a single layer HDRA with $\epsilon_r = 10$.

To sum up, high gains have been acquired for both lower and higher DRA permittivities, albeit with a wider bandwidth and approximately half the size in the latter case. In addition, although the smaller DRA offers almost doubled bandwidth, it is still relatively narrow to meet the requirements of the high data rates in 5G communication systems. This drawback will be addressed in the next section.

3.2. Two-Layer HDRA

A lower permittivity dielectric coat has been incorporated in the proposed hemispherical DRA of Subsection 3.1 in order to enhance the impedance bandwidth, while maintaining a high gain. A cross-slot has been utilized again to feed the two-layer hemispherical DRA configuration as illustrated in Fig. 4, where the inner and outer layers permittivities have been chosen based on the availability of the
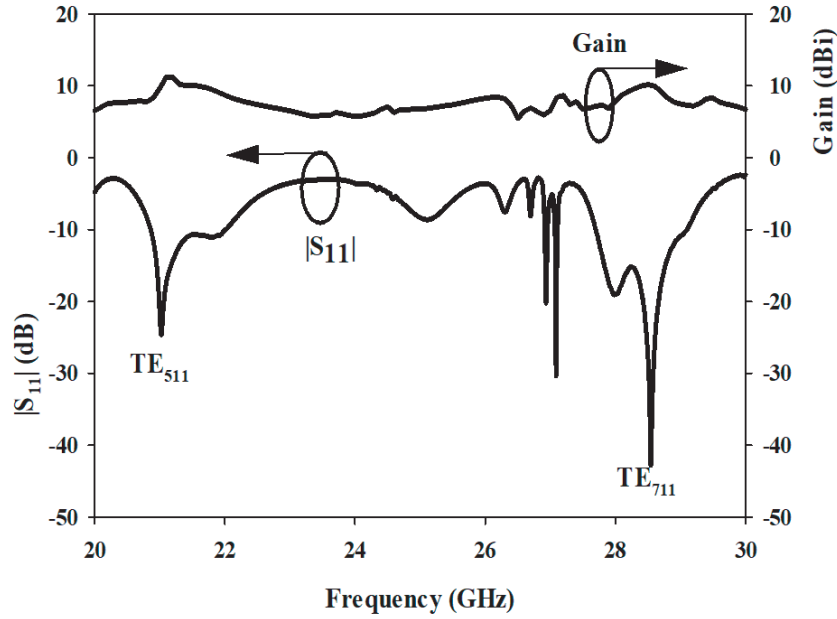
Figure 3. Simulated S-parameters and gain of a single layer hemispherical DRA when $\epsilon_r = 20$.
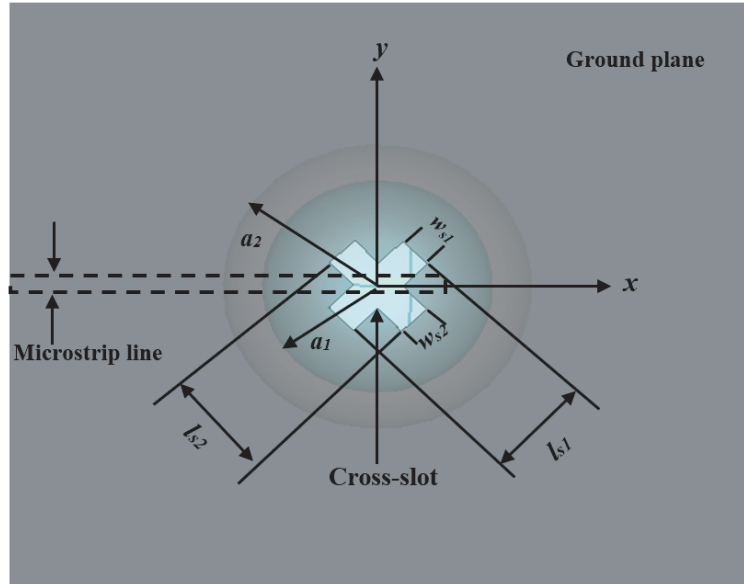

Figure 4. Two-layer HDRAs fed by cross-slot.

dielectric materials. The length of stub and the slots lengths and widths are optimized using CST MWS to ensure a maximum coupling between the antenna and its feed network as can be observed in Table 1. In addition, to acquire a further understanding of the outer layer's impact, the effective permittivity of the DRA is calculated as [20]

$$\epsilon_{r1,2} = \epsilon_{r2} \frac{a_2^3(\epsilon_{r1} + 2\epsilon_{r2}) + 2a_1^3(\epsilon_{r1} - \epsilon_{r2})}{a_2^3(\epsilon_{r1} + 2\epsilon_{r2}) - a_1^3(\epsilon_{r1} - \epsilon_{r2})} \tag{1}$$

Moreover, with reference to Table 1 and Fig. 5, it can be observed that for a hemispherical DRA with $\epsilon_{r1} = 10$ that is coated by an outer layer of $\epsilon_{r2} = 3.5$, the effective permittivity of the configuration
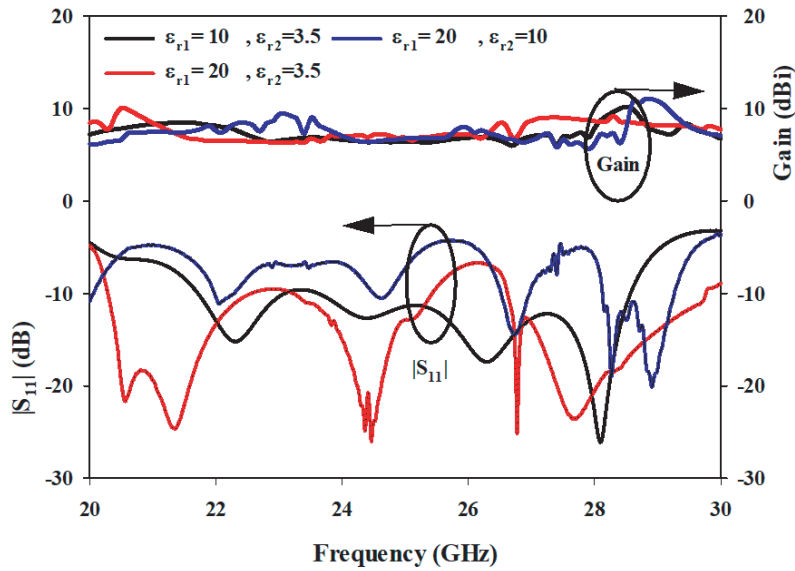
Figure 5. Reflection coefficient for various dielectric constants of the inner and outer layers of the proposed HDRA.

is reduced to 5.5. The lower effective permittivity provides a wider impedance bandwidth of 18.8% with lower gain and larger size than that of a DRA with $\epsilon_{r1} = 20$. On the other hand, increasing ϵ_{r1} to 20 provides a higher gain with a lower impedance bandwidth due to the higher effective permittivity. It should be pointed that using a material with $\epsilon_{r2} = 3.5$ as a coat for a hemispherical DRA of $\epsilon_{r1} = 20$ reduces the reflections at the coat-air interface, while maintaining strong wave reflections at the coat-DRA interface due to the considerable differences in the two materials' permittivities. Similarly, coating the same DRA with a layer of Alumina, $\epsilon_{r2} = 10$, reduces the wave reflections at the DRA-coat interface albeit with stronger reflections at the coat-air interface. As a result, utilizing a DRA with $\epsilon_{r1} = 20$ combined by a coat layer of $\epsilon_{r2} = 3.5$ improves the bandwidth and reduces the gain compared to that of a single layer DRA. On the other hand, if the same DRA is coated by a material with $\epsilon_{r2} = 10$, then higher gain with narrower impedance bandwidth are achieved. This can be explained in terms of the effective permittivity as illustrated in Table 1, where it can be noted that increased gains are combined with narrower bandwidths and achieve lower effective wavelengths corresponding to effectively larger electrical DRA size. Therefore, a multiple coat layers configuration needs to be considered in order to accomplish a high gain wide-band hemispherical DRA. The multi-layer coat acts as a multi-stage transition region between free space and the DRA element with minimised wave reflections at all dielectric interfaces. The three layers DRA configuration is investigated in the next section.

3.3. Three-Layer HDRA

For studying the characteristics of the proposed three-layer hemispherical dielectric resonator antenna, the investigation has been performed for different third layer thicknesses as illustrated in Table 2. It is worth pointing that the thicknesses of the first and second layers have been initially fixed at 4.5 and 6 mm with respective relative permittivities of 20 and 10. This is because the maximum gain 11 dBi has been achieved using those parameters as illustrated in Table 1. Once again, the effective permittivity of the three layers has been calculated as [21],

$$\epsilon_e = \epsilon_{r3} \frac{a_3^3(\epsilon_{r1,2} + 2\epsilon_{r3}) + 2a_2^3(\epsilon_{r1,2} - \epsilon_{r3})}{a_3^3(\epsilon_{r1,2} + 2\epsilon_{r3}) - a_2^3(\epsilon_{r1,2} - \epsilon_{r3})} \tag{2}$$

From Table 2 and Fig. 6 it can be observed that as the outer layer thickness increases, the effective permittivity is reduced, which provides a maximum impedance bandwidth in conjunction with a gain of 9.5 dBi when $a_3 = 8$ mm, with an effective permittivity of 6.22. However, lower effective permittivity can

Table 1. Comparison of the performances of various layered hemispherical DRA configurations with different ϵ_{r1} and ϵ_{r2}.

Dielectric constant		Radius (mm)		Stub length (mm)	Slots' dimensions $l_s \times w_s$ (mm^2)	Gain (dBi)	Impedance bandwidth %	ϵ_{eff}	λ_{eff} at 28 GHz (mm)
ϵ_{r1}	ϵ_{r2}	a_1	a_2						
10	1	11	-	1	4×1.35	10.7	2.7	10	3.33
10	3.5	4.5	10	1	2.7×1.35	7	18.8	5.5	4.56
20	1	4.5	-	1.25	4×1.35	10	5.46	20	2.4
20	3.5	4.5	6	1.25	4×1.35	8.2	11.1	7.14	4
20	10	4.5	6	1.25	4×1.35	11	4	13.5	2.91

Table 2. Comparison of the performances of various layered hemispherical DRA configurations with different ϵ_{r1} and ϵ_{r2}.

Three-layer HDRA radii (mm)			ϵ_{eff}	λ_{eff} at 28 GHz (mm)	Impedance bandwidth (%)	Gain (dBi)
a_1	a_2	a_3				
4.5	6	6.5	10	3.38	3.5	8
4.5	6	7	8.16	3.75	12.5	10.6
4.5	6	7.5	7	4.04	20	10.3
4.5	6	8	6.22	4.3	35.8	9.5
4.5	6	8.5	5.6	4.52	18.2	8.5

be achieved for a thicker outer layer but with deteriorated bandwidth and gain, which may be attributed to the change in the effective dimensions of the cross-slot and matching stub. From these results it can be noticed that a maximum gain of 10.6 dBi has been achieved when $a_3 = 8$ mm in conjunction with narrower impedance bandwidth of 12.5%. Therefore, a thickness of $a_3 = 8$ mm has been chosen for the measurements as it provides the best trade-off between the impedance bandwidth and gain.
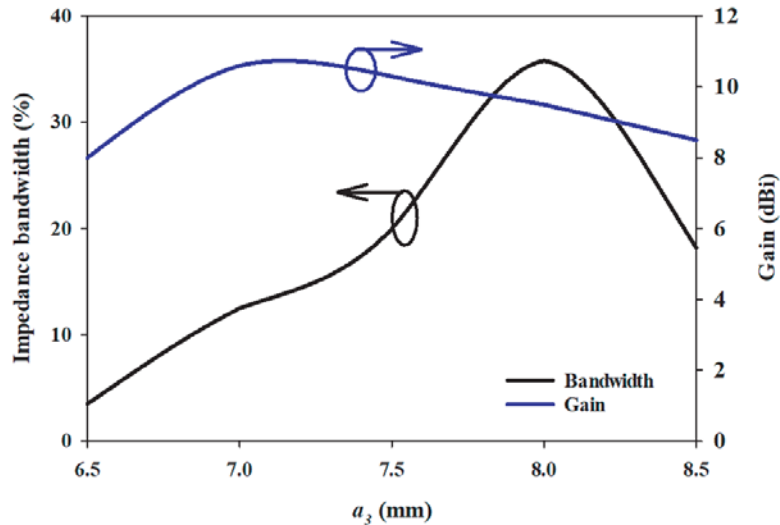
Figure 6. Impedance bandwidth and gain as functions of the third layer thickness.

4. MEASUREMENTS PROCEDURE

A prototype of the optimized three layers hemispherical DRA has been built and measured. The inner two layers have been fabricated using E-20 ceramic and Alumina provided by T-Ceram, while the outermost layer has been fabricated using 3D printing technology at the University of Sheffield utilising a polyamide material (N12). The respective layers' radii have been chosen as $a_1 = 4.5$ mm, $a_2 = 6$ mm, and $a_3 = 8$ mm. The antenna has been excited by etching a cross-slot aperture in the metal ground plane. In order to ensure optimum matching, the open stub length has been chosen as $l_{stub} = 1.25$ mm, and a microstrip line width of 0.5 mm has been utilised. It should be noted that the first and second layers have been fabricated with a precision of 5% compared to 1% for the third layer. The antenna has been placed on a 25 mm^2 ground plane with a thickness of 0.4 mm. The feed network has been provided by Wrekin Circuit Ltd, where the substrate has been fabricated using Rogers RO4003C with relative permittivity of 3.5. The layered DRA prototype has been mounted on the ground plane, with the aid of a double-sided adhesive copper tape in order to eliminate the potential air-gaps and keep the antenna stable with respect to the feed network. Otherwise, the antenna may be shifted due to the smaller size and lighter weight. The S parameters have been measured using E5071C vector network analyser through a 50 Ω coaxial cable. In addition, a 2.92 mm SMA has been utilized between the coaxial cable and the feeding strip line. The calibration has been carried out using the Agilent's 85052D calibration kit. The radiation patterns have been measured using the SNF-FIX-1.0 Spherical Near-field mm-Wave Measurement System. In order to measure the antenna gain, the well-known comparison procedure has been adapted in which a reference horn antenna has been used at the receiving end, where the DRA gain has been determined as [21].

$$G_{\text{DRA(dB)}} = G_{\text{Horn(dB)}} + 10 \log_{10} \left(\frac{P_{\text{DRA}}}{P_{\text{Horn}}} \right) \tag{3}$$

5. EXPERIMENTAL RESULTS

The fabricated prototype of the layered hemispherical DRA is presented in Fig. 7 and placed on the feed network as illustrated in Fig. 8. The measured and simulated reflection coefficients are presented in Fig. 9, where it can be noted that the results correlate well with each other. For example, a simulated bandwidth of 35.8% has been achieved over a frequency range of 20.8 to 29.9 GHz, compared to a measured counterpart of 35.5% over a frequency range of 20.5 to 29.4 GHz. Furthermore, as the hemispherical DRA layers are physically small, measurements errors are expected to some extent. As a

Figure 7. Prototype of a multi-layer mm-wave hemispherical DRA before and after assembly.

(a)   (b)

Figure 8. Geometry of three-layer HDRA placed on feed network (a) Top view, (b) bottom view.
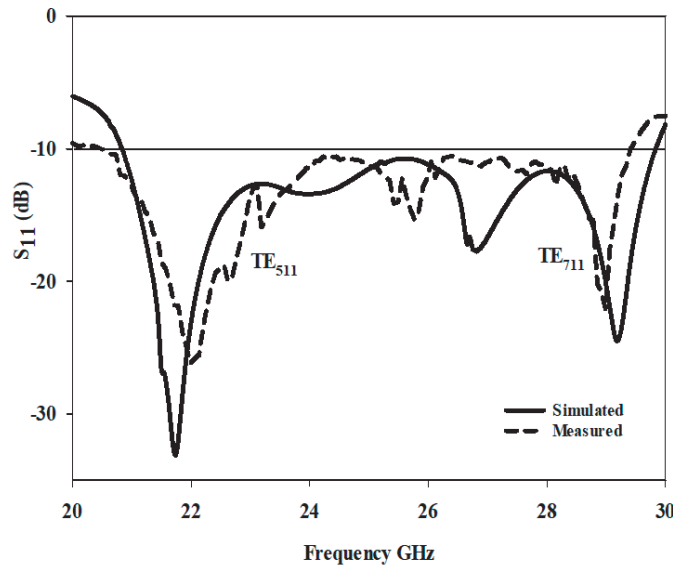

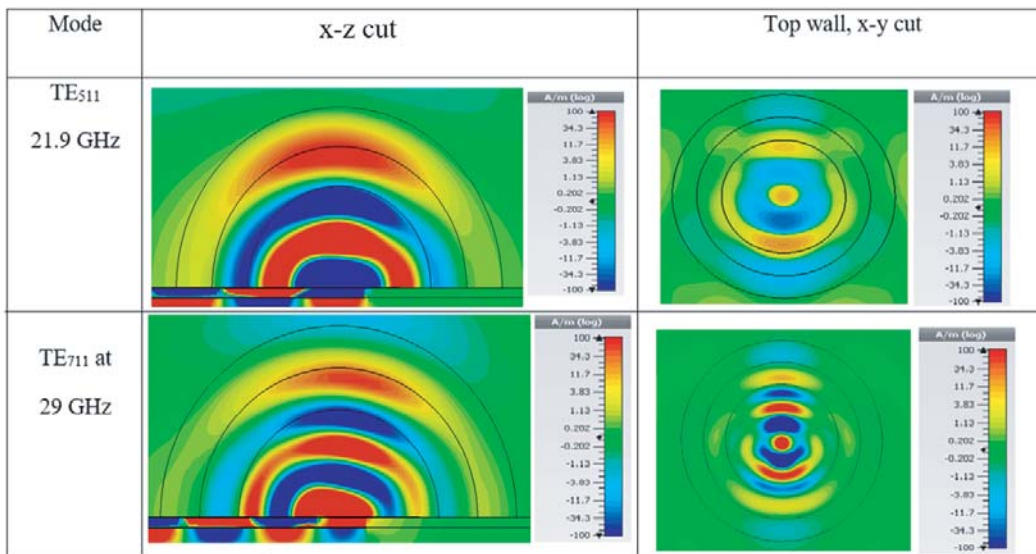**Figure 9.** Reflection coefficient of a three-layer hemispherical DRA.

Figure 10. Magnetic field distribution inside the three layers hemispherical DRA for the TE_{511} and TE_{711} resonance modes.
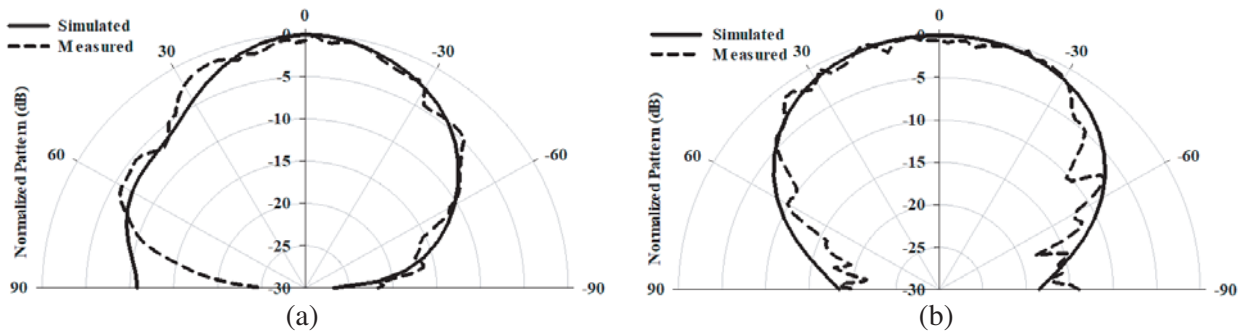
Figure 11. Radiation patterns of mm-wave HDRA excited in the TE_{511} mode at 21.9 GHz. (a) $\phi = 0°$, (b) $\phi = 90°$.
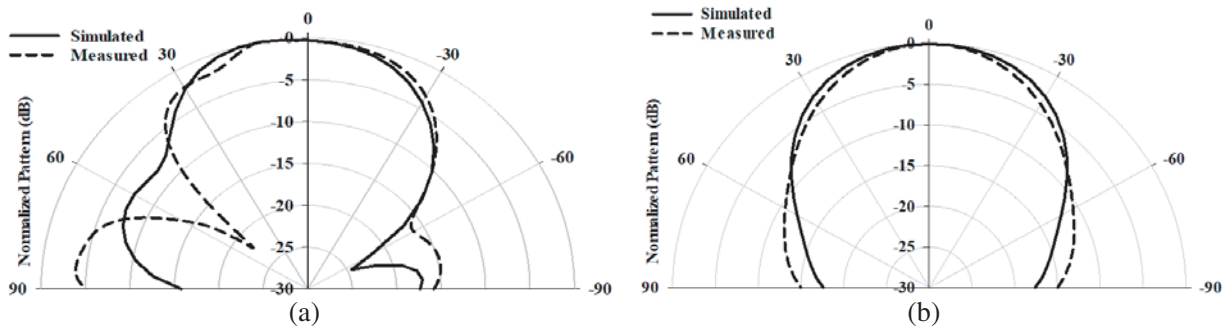

Figure 12. Radiation patterns of mm-wave HDRA excited in the TE_{711} mode at 29 GHz. (a) $\phi = 0°$, (b) $\phi = 90°$.

result, a slight frequency shift has been noted in the reflection coefficient measurements. The magnetic field distribution inside the three layer hemispherical DRA is presented in Fig. 10, where it can be observed that the proposed DRA supports the TE_{511} and TE_{711} higher order modes. The simulated and measured radiation patterns are depicted in Fig. 11 and 12 for both of the principle E and H planes at 21.9 and 29 GHz, respectively. Reasonable agreement has been achieved between experimental and simulated far fields with minor degradation at the E-plane side-lobes that could be attributed to the measurements and fabrication tolerances. For example, the SMA connector and soldering, which have not been considered in the simulations, become electrically large at higher frequencies and act as an

Table 3. Comparison between the proposed high gain wide bandwidth HDRA and previously proposed designs.

References	Number of layers	Overall size (λ_0)	Frequency range (GHz)	Gain (dBi)	Bandwidth (%)
Proposed antenna	Three	0.6	21-30	9.45	35.8
[9]	Three	0.48	7.5–10.8	-	55
[10]	Three	0.5	5.1–7.42	3.28	65.6
[11]	Three	0.72	8.4–9.5	6.4	9.6
[12]	Three	0.25	2.8–3.25	-	25.79
[13]	Three	0.45	4.5–6.5	4.5	36
[14]	Two	0.35	2.8–3.9	2.5	31.9

effective scatterer that degrades the radiation patterns [22]. It is worth pointing that asymmetric curves for $\phi = 0°$ and $\phi = 90°$ could be attributed to the asymmetrical magnetic field distribution in the xz plane due to loading the DRA with the feed network as can be observed from Fig. 10. Furthermore, close agreement has been achieved between measured and simulated gains as demonstrated in Fig. 13. It is worth mentioning that the simulated radiation efficiency of the DRA is more than 90% over the considered frequency range. However, it has been noted to be slightly lower during the measurements due to the presence of SMA, soldering, and loss in the cables. A comprehensive comparison between the performances of the proposed antenna and those reported in the literature is tabulated in Table 3, where it can be observed that even though the proposed design is slightly larger, the DRA combines the benefits of higher gain and wider bandwidth, which outperforms the earlier deigns that generally offer wider bandwidth in conjunction with lower gain. Therefore, it can be concluded that the first mm-wave hemispherical DRA has been reported with a gain that considerably exceeds those of the reported lower frequencies counterparts while maintaining a wideband operation.
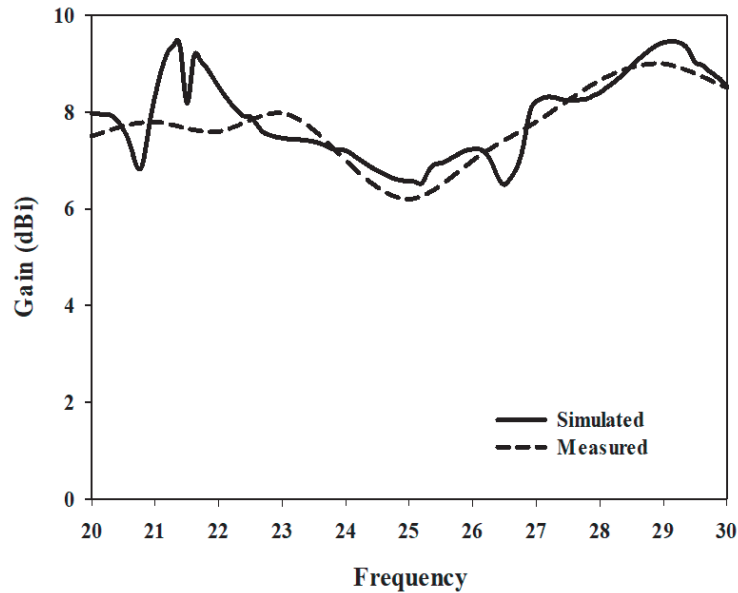

Figure 13. Simulated and measured gain of three-layer hemispherical DRA.

6. CONCLUSIONS

The operation of an mm-wave higher order mode hemispherical DRA has been investigated and demonstrated experimentally. As expected, the fundamental and lower order hemispherical DRA modes operation offers lower gain due to the broad beam-width that results from the nature of the magnetic field distribution throughout the hemispherical DRA. In order to increase the gain, extremely high order resonance modes need to be excited, which requires considerably larger DRA dimensions. As a result, higher dielectric constants may be considered as an option to maintain a practical DRA size while improving the gain. However, the combinations of higher DRA dielectric constants with higher order mode operation result in an extremely narrow bandwidth. Therefore, multiple coat layers have been proposed in order to provide multi-stage transition regions between free space and the DRA element with minimised wave reflections at all interfaces. As a result of incorporating two outer layers, the impedance bandwidth has been improved to 35.8% with a maximum gain of 9.45 dBi. This represents the highest gain reported for a single hemispherical DRA, and previously such gain could only be achieved with DRA arrays, which increases size, complexity, and losses. In addition, the outer layer provides a physical support to the smaller size HDRA element. Furthermore, close agreement between simulated and measured results has been accomplished.

REFERENCES

1. Kim, J. G., H. S. Lee, H. S. Lee, J. B. Yoon, and S. Hong, "60-GHz CPW-fed post-supported patch antenna using micromachining technology," *IEEE Microwave & Wireless Components Letters*, 2005.

2. Garcia, C. R., R. C. Rumpf, H. H. Tsang, and J. H. Barton, "Effects of extreme surface roughness on 3D printed horn antenna," *Electronics Letters*, Vol. 49, 734–736, 2013.

3. Petosa, A. and S. Thirakoune, "Design of a 60 GHz dielectric resonator antenna with enhanced gain," *IEEE Antennas and Propagation Society International Symposium (APSURSI)*, 1–4, 2010.

4. Nor, N. M., M. H. Jamaluddin, M. R. Kamarudin, and M. Khalily, "Rectangular dielectric resonator antenna array for 28 GHz applications," *Progress In Electromagnetics Research C*, Vol. 63, 53–61, 2016.

5. Gangwar, R. K., S. P. Singh, and D. Kumar, "Comparative studies of rectangular dielectric resonator antenna with probe and microstrip line feeds," *Archives of Applied Science Research*, Vol. 2, 1–10, 2010.

6. Petosa, A. and S. Thirakoune, "Rectangular dielectric resonator antennas with enhanced gain," *IEEE Transactions on Antennas and Propagation*, Vol. 59, 1385–1389, 2011.

7. Abdulmajid, A. A., Y. Khalil, and S. Khamas, "Higher-order-mode circularly polarized two-layer rectangular dielectric resonator antenna," *IEEE Antennas and Wireless Propagation Letters*, Vol. 17, 1114–1117, 2018.

8. Abdulmajid, A. A. and S. Khamas, "Higher order mode layered cylindrical dielectric resonator antenna," *Progress In Electromagnetics Research C*, Vol. 90, 65–77, 2019.

9. Leung, K. W. and K. K. So, "Theory and experiment of the wideband two-layer hemispherical dielectric resonator antenna," *IEEE Transactions on Antennas and Propagation*, Vol. 57, 1280–1284, 2009.

10. Kakade, A. B. and B. Ghosh, "Mode excitation in the coaxial probe coupled three-layer hemispherical dielectric resonator antenna," *IEEE Transactions on Antennas and Propagation*, Vol. 59, 4463–4469, 2011.

11. Kakade, A. B. and B. Ghosh, "Analysis of the rectangular waveguide slot coupled multilayer hemispherical dielectric resonator antenna," *IET Microwaves, Antennas & Propagation*, Vol. 6, 338–347, 2012.

12. Kakade, A. B. and M. S. Kumbhar, "Wideband circularly polarized conformal strip fed three layer hemispherical dielectric resonator antenna with parasitic patch," *Microwave and Optical Technology Letters*, Vol. 56, 72–77, 2014.

13. Ghosh, B. and A. B. Kakade, "Mode excitation in the microstrip slot-coupled three-layer hemispherical dielectric resonator antenna," *IET Microwaves, Antennas & Propagation*, Vol. 10, 1534–1540, 2016.

14. Fang, X. S. and K. W. Leung, "Design of wideband omnidirectional two-layer transparent hemispherical dielectric resonator antenna," *IEEE Transactions on Antennas and Propagation*, Vol. 62, 5353–5357, 2014.

15. Leung, K. W., K. M. Luk, K. Y. Lai, and D. Lin, "Theory and experiment of an aperture-coupled hemispherical dielectric resonator antenna," *IEEE Transactions on Antennas and Propagation*, Vol. 43, 1192–1198, 1995.

16. Leung, K. W., K. W. Ng, K. M. Luk, and E. K. N. Yung, "Simple formula for analysing the centre-fed hemispherical dielectric resonator antenna," *Electronics Letters*, Vol. 33, 440–441, 1997.

17. Luk, K. M. and K. W. Leung, "Dielectric resonator antennas research studies press limited," 2002.

18. Microwave Studio, "Computer simulation technology (CST)," Online: www.cst.com, 2015.

19. Gregson, S., J. Mc Cormic, and C. Parini, "Principles of planar near-field antenna measurements," *The Institute of Engineering and Technology*, 2007.

20. Abdulmajid, A. A., S. Khamas, and S. Zhang, "Wide bandwidth high gain circularly polarized millimetre-wave rectangular dielectric resonator antenna," *Progress In Electromagnetics Research*, Vol. 89, 171–177, 2020.

21. Chettiar, U. K. and N. Engheta, "Internal homogenization: Effective permittivity of a coated sphere," *Optics Express*, Vol. 20, 22976–22986, 2012.

22. Pan, Y. M., K. W. Leung, and K. M. Luk, "Design of the millimeter-wave rectangular dielectric resonator antenna using a higher-order mode," *IEEE Transactions on Antennas and Propagation*, Vol. 59, 2780–2788, 2011.